MICROMECHANICAL ASPECTS OF TRANSGRANULAR AND INTERGRANULAR FAILURE COMPETITION

I. Dlouhy, H. Hadraba and M. Holzmann
Institute of Physics of Materials, Academy of Sciences of the Czech Republic,
Žižkova 22, 61662 Brno
Czech Republic

ABSTRACT

Main purpose of the work was to quantify causes and characteristics that control the intergranular fracture initiation and occurrence of this fracture micromechanism in competition with cleavage one. A CrNi steel of commercial quality and the same steel with increased content of impurity elements, Sn and Sb, have been used for investigation. Step cooling treatment was applied in order to induce intergranular embrittlement and brittle fracture initiation in both steel melts. For fracture toughness determination standard bend specimen geometry and the pre-cracked Charpy type specimens both tested in three point bending were applied for determination of fracture mechanical properties. Relation of cleavage fracture stress and critical stress for intergranular failure has been followed showing capability of this parameter for quantification of the transgranular/intergranular fracture. In order to characterise the quantitative morphological differences in fracture surfaces fractal analysis was applied. A boundary level of fracture dimension has been determined to be 1.12 for the investigated steel, the fracture surface roughness higher than the value reflects high level of intergranular embrittlement and thus fracture toughness degradation.

Introduction

Occurrence of intergranular initiation of brittle fracture could be taken as significant simple measure of the negative influence of impurities content. This micromechanism of failure has been usually responsible for strong decrease of mechanical properties, anomalous fracture behaviour or, at least, comparably larger and in structural applications unacceptable data scatter [1-4].

In embrittlement of technological nature - heat affected zones, overheated microstructures etc. - impurities atoms are attracted to grain boundaries causing their weakening [5]. Usually, these changes are associated with intergranular fracture micromechanism as result of embrittlement. In weld metal very specific role of inclusion in cleavage fracture is often assessed as the inclusion triggered cleavage may strongly overlap an inherent metal toughness in many cases [6,7].

In embrittlement due to long term thermal exposition two micromechanisms control the changes in fracture micromechanism: (i) temper embrittlement caused by growth of carbide diameter leading to change of transgranular cleavage from dislocation triggered to carbide induced [8,9]. (ii) intergranular embrittlement caused by contemporary effect of diffusion of impurities and carbide coarsening at grain boundaries and/or interface boundaries [2,3 etc.].

The intergranular fracture initiation itself has to be taken as result of competition between two stress-controlled fracture micromechanisms: cleavage and intergranular. For action of these micromechanisms a criterion of some local fracture stress acting over some microstructurally susceptible distance (volume) has to be reached. What is the cause that forces the metal grain boundary to fail in intergranular manner rather than transgranular? As known, it is a cohesion strength that decreases at the same time as the cleavage fracture stress is kept on the same level. But a number of questions are connected with relation of microscopic cohesion strength and local fracture stress, with effect of pre-strain due to cold deformation or constraint phenomena etc. An interconnection of fractographic methods with analysis of data from simple suitable specimen (e.g. Charpy type) seems to be the effective tool for solution of these problems.

The aim of paper can be seen in analysis of micromechanical aspects of brittle fracture initiation connected with intergranular decohesion as micromechanism that is well susceptible to metallurgic cleanliness and cumulative degradation of material. Causes and characteristics governing the intergranular fracture initiation and occurrence of this fracture micromechanism in competition with cleavage one should be also addressed.

Experimental

Material characteristics. Two different melts of CrNi pressure vessel steel have been used having the chemical composition shown in table 1.

Table 1. Chemical compositions of steel melts used in investigation (in wt %)

Melt designation	C	Mn	Si	Cr	Ni	S	P	Sn	Sb	As
A (as received)	0.15	0.40	0.21	0.72	3.51	0.011	0.010	0.003	0.005	0.002
R (remelted)	0.20	0.45	0.145	0.74	3.57	0.013	0.011	0.014	0.036	0.005

The steel melt A has been received as commercially produced hot rolled bar having rectangular section 80x80 mm^2. The impurities content in this steel was qualified as common. The steel melt R has been prepared from the melt A by remelting in atmospheric induction furnace doping the melt by Sn and Sb (table 1).

The following microstructural states have been prepared for investigation in both these steel melts: (i) standard (ferritic) microstructure (state obtained by normalisation treatment from 940 °C with quenching into water and tempering at 650 °C for about 100 h), and (ii) ferritic microstructure in embrittled conditions (the same microstructure as in case (i) additionally thermally aged). The embrittling ageing applied was either isothermal (IA) at 550°C for 150 h or so called step-cooling regime (SC – as shown in work [10]).

Selected materials characteristics are shown in Table 2. In this table, the value of d_F represents ferritic grain size. Basic mechanical properties shown here were obtained at room temperature. Fracture appearance transition temperature (*FATT*) has been introduced here as characteristics describing the location of transition region on temperature axis for the steel microstructures investigated.

Table 2. Microstructural and selected mechanical characteristics of materials studied

Microstructure labelling	Thermal exposition	d_F [µm]	$R_{p0.2}$ [MPa]	R_m [MPa]	CVN imp. energy [J]	*FATT* [°C]
A	initial state	16	490	621	260	-80
A & IA	isotherm al	18	510	658	210	-75
A & SC	step cooling	17	508	652	205	-60
R	initial state	17	485	605	156	-40
R & SC	step cooling	19	496	632	85	+25

Mechanical testing. The yield strength and other tensile properties including true stress - true strain curves have been measured using cylindrical specimens with diameter of 6 mm and gauge length 25 mm being loaded over temperature range of -196 to +200 °C at the cross-head speed of 2 $mm.min^{-1}$.

For steel melt A the temperature dependencies of fracture toughness have been measured using standard 25 mm thick specimen loaded in three point bending at the cross-head speed of 1 $mm.min^{-1}$. Standard procedures have been applied for fracture toughness determination. For both steel melts, A and R, pre-cracked Charpy type specimens have been also applied for the fracture toughness tests because of limited amount of experimental steel R. The standard fracture toughness temperature diagrams have been evaluated by means of master curve methodology [11].

Temperature dependencies of CVN impact energy were measured statically and dynamically. Fracture appearance transition temperatures (*FATT*) have been determined among others. To evaluate the local fracture stress, s_f, the load - displacement traces have been recorded, and the maximum force, fracture force, and general yield force, respectively have been taken from records and plotted against temperature. For one selected temperature below t_{gy}, temperature where fracture and general yield force were coincident, a range of bend tests was performed to obtain data for statistical treatment for all microstructures tested. The details of the analyses are available in [10].

Fractography and supporting procedures. For CVN specimens tested around and below the brittleness transition temperature, t_{gy}, the distances of the fracture initiation sites from the notch root were evaluated using SEM micrographs. To identify the microstructural causes of cleavage facet nucleation the triggering origins of facets in failure initiation sites were assessed. Similar procedures were applied in order to prove the correlation of intergranular facets with ferritic grain size.

Fractal dimension analysis was carried out in order to characterise the fracture surfaces quantitatively. The method principles have been in detail described elsewhere [12]. The value of fractal dimension, D_F, has been determined from metallographic sections perpendicular to fracture in direction of crack propagation. Dependences of D_F on distance from the crack tip has been analysed in mentioned paper, the mean value corresponding to brittle fracture morphology was used for purposes of this work.

For test temperature below general yield temperature, t_{gy}, (see table 3) the principal stress distributions below the notch were calculated. A 3D approach was developed for the elastic-plastic analysis. Standard finite element computer code ABAQUS was used for these purposes.

Analysis of the Results

Fracture toughness and fracture performance of the steel. The typical temperature dependence of fracture toughness (FTTD) is shown in Figure 1 for the steel A in initial state. In order to determine the scatter band of fracture toughness values in the transition and lower shelf regime a number of specimens was tested at one temperature and data obtained are also given in the figure. For purposes of comparison with other microstructural states investigated the validity of master curve methodology was proved. The master curve is represented by full line; the 90 % probability scatter band is shown by dashed curves. The transition from cleavage to ductile fracture initiation is represented in figure by temperature t_{DBL} that is the lowest temperature leading to brittle fracture with some ductile tearing. The ductile tearing preceding the cleavage was determined fractographically and has been indicated by symbols K_{Ju} and K_{Jm} in the Figure 1.

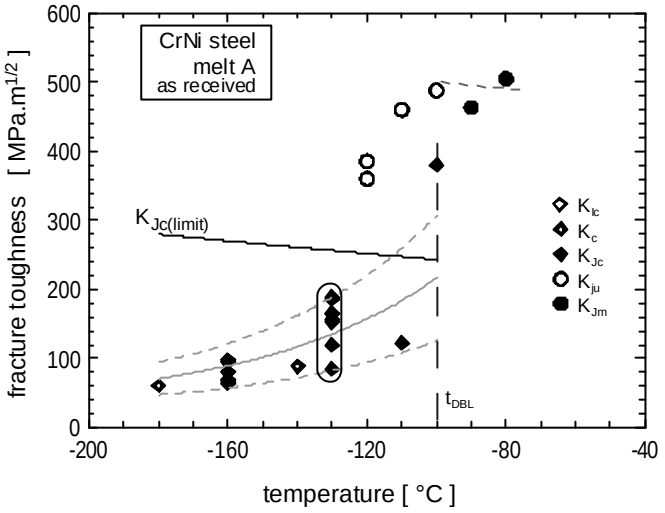

Figure 1. Fracture toughness temperature diagram for the steel with initial microstructure

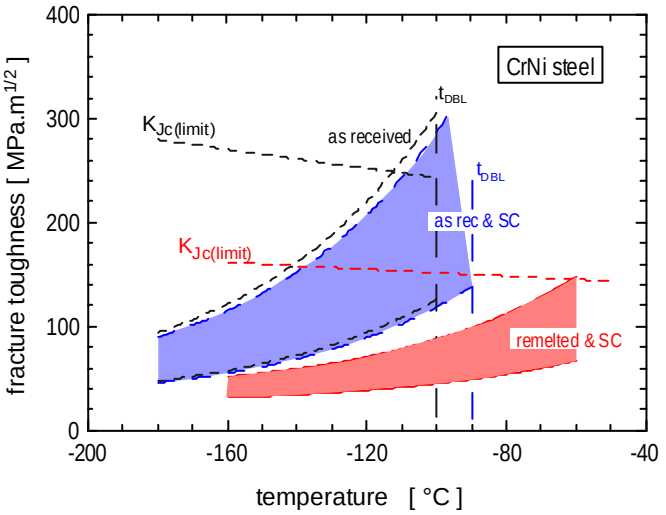

Figure 2.Comparison of FTTD for both steel melts after step cooling treatment

Similar approach has been chosen for the other states of the steel. The following Figure 2 thus shows the fracture properties for steels A and R after step-cooling treatment (SC). Both states are represented by scatter band limited by red dashed and blue full line respectively. The as received state is in the figure represented by black thin dashed lines only. It follows from comparison of main trends that except for the scatter in fracture toughness values a very limited embrittlement occurred and only slight shift of transition region was observed for melt A after step cooling.

No extensive intergranular fracture was identified in fracture surfaces as shown in Figure 3. Almost transgranular cleavage can be seen in fracture surfaces. Some grain boundaries embrittlement occurred however; the evidences can be seen in secondary microcracks oriented perpendicularly to major crack and usually in triple points of initial grain boundaries. It follows from the Figures 2 and 3 that it is practically impossible to produce by applied ageing procedures more extensive (intergranular) embrittlement in steel A (in a fine-grained microstructure of this steel). The change in fracture toughness and fracture behaviour is practically so low, that no remarkable embrittlement took place. Detailed analyses of metallographic section have shown (after etching in picric acid) that enrichment of grain boundaries by impurity elements did occur.

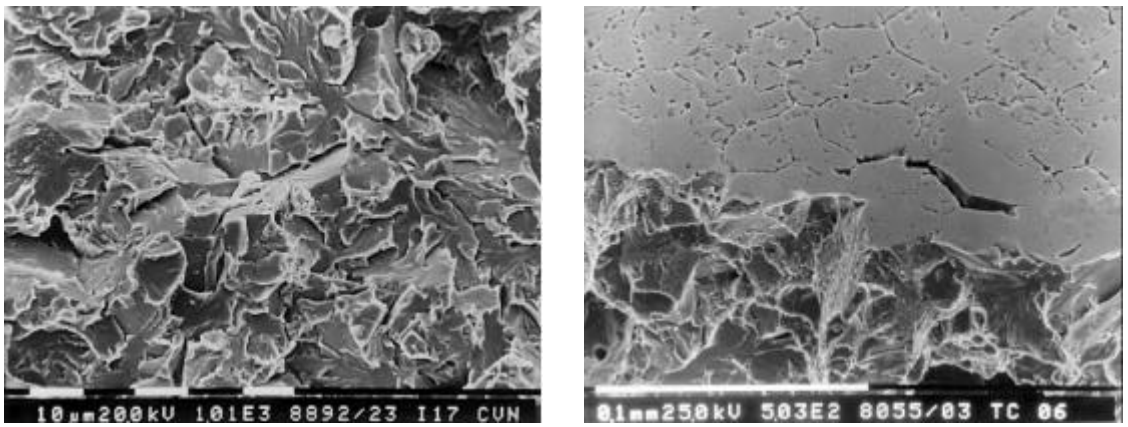

Figure 3. Example of fracture surface of the melt A after step cooling treatment (left) and metallographic section perpendicular to fracture surface (right)

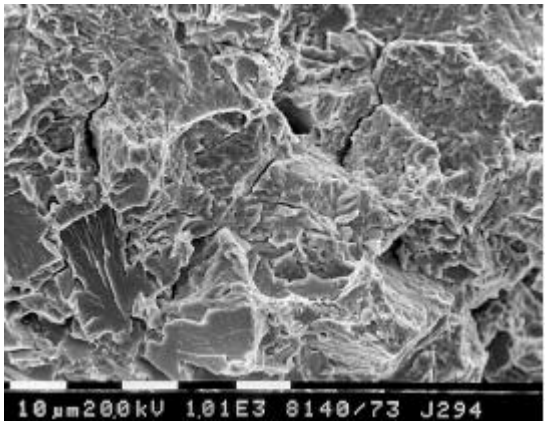

Figure 4. Example of fracture surface of the melt R after step cooling treatment

For melt R after step cooling treatment the fracture appearance of pre-cracked specimen tested in lower shelf region is obvious from Figure 4. More than 60 % of intergranular fracture was observed. In connection with the shift of transition region to much higher temperatures, with the shift of transition for CVN impact energy [10] - (see also the *FATT* in Table 2) and with the significant decrease of fracture toughness in lower shelf and transition region the detrimental impurity content at grain boundaries is clearly obvious.

Quantitave characterisation of fracture surfaces. Several experimental approaches of fractal dimension determining were followed extensively in order to generate the representative quantification of the fracture morphology [12]. The metallographic

sections perpendicular to fracture plane in direction of crack propagation has been found as the most representative. For calculation of fractal dimension D_F the Richardson's formula has been applied having after the mathematical derivation the following form:

$$D_F = 1 - \frac{d \log R_L}{d \log h} ,$$

where R_L is the roughness parameter of fracture profile and h is the length of the yardstick. The fractal dimension was acquired from the empirical measurement of the fracture profile as the slope of a linear regression dependence $\log R_L$ vs $\log h$. The length size of the yardstick depends on proportions of characteristic units, out of which the fracture surface is composed. The smallest length of yardstick was h = 3.4 μm.

The Figure 5 shows part of results. First of all, the separate values represent data obtained for steel A in initial state (black empty circles) and in embrittled state (blue rhombi). Except for separate data the scatter bands are shown for initial state represented by full black lines only, for the state after embrittling ageing by blue shaded field. It follows from comparison that practically the same values of fractal dimension appear to be the main characteristics of brittle failure for both microstructures - initial (A) and embrittled (A&SC). Based on this finding and based on knowledge shown in previous part, the "embrittled" state of steel A posses still acceptable properties and embrittlement process is just in first stages of conversion to intergranular initiation. On the other side evident differences have been found when comparing both embrittled microstructures of the steel melt A and R - compare the both shaded fields, blue for steel A and red for steel R, both after step cooling to induce embrittlement. The higher value of fractal dimension corresponds to higher fracture roughness due to intergranular failure mechanism (for comparisons see also the values of fractal dimension D_F shown in Table 3).

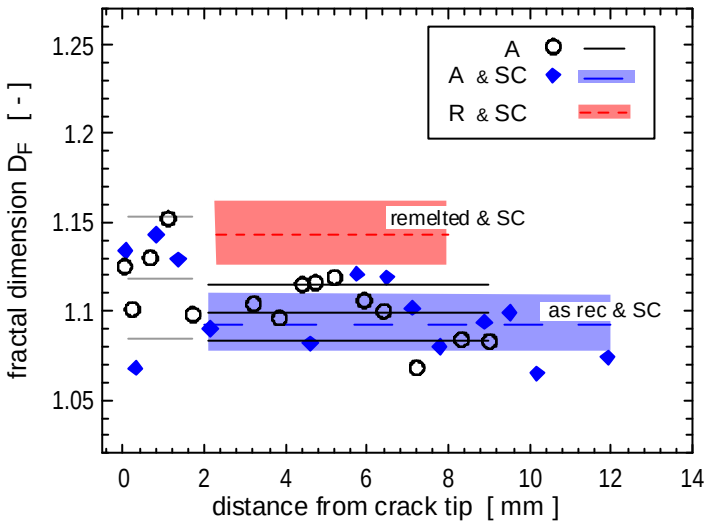

Figure 5. Change of fractal dimension, D_F, with distance from crack tip

As it has been analysed in other our work [13] a boundary between transgranular and intergranular micromorphology of the fracture surface can be quantified through the value of fractal dimension. Based on statistically meaningful amount of data the limit value of D_F = 1.12 has been obtained. This value of fractal dimension can be taken as a measure of the steel embrittlement.

In addition, the dependence of fractal dimension on distance from the crack tip possesses regular oscillations that could be joined with crack propagation dynamics [10] and periodic features in fracture surfaces.

Figure 6 shows summarisation of set of data obtained from selected area of fracture surface of precracked specimen (steel R after step cooling treatment). The D_F values from separate metallographic sections perpendicular to fracture surface are here plotted as a function of specimens thickness and distance from the crack tip. The D_F values higher than the limit value 1.12 are plotted in red, the value lower than this boundary are in shown in blue. The discrete values have been fitted by smoothed curves in order to visualize the changes in fractal dimensions as continuous relief using 3D graphic software (surfer). The red "peaks" thus represent area with increased roughness (i.e. higher fractal dimension) that is connected with intergranular failure mechanism.

Once having the boundary value between intergranular and transgranular fracture for the given steel similar fractal analysis can be carried out giving figure about the level of intergranular embrittlement.

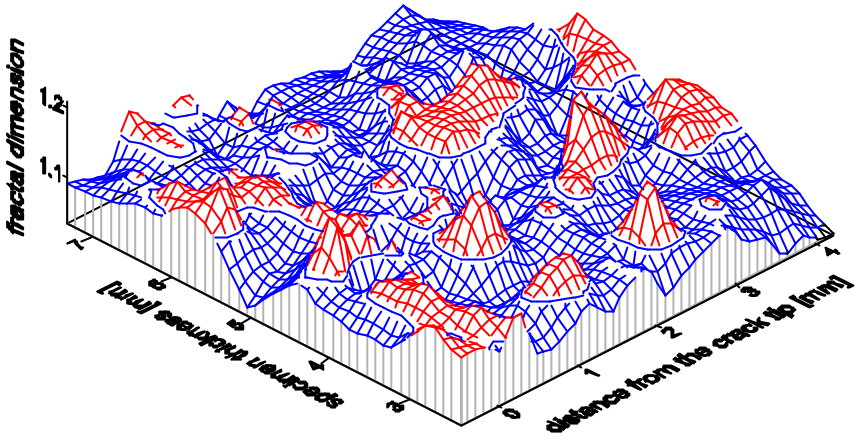

Figure 6. 3D visualization of fractal dimension in steel R after step cooling – dependence of D_F on specimen thickness and distance from the crack tip.

Critical (fracture) stress quantification. To determine the local fracture stress experimentally two procedures were used:

(i) For CVN specimens loaded statically and/or dynamically, at temperatures where the fracture and general yield forces were coincident, the local maximum tensile stress was calculated taking the value of 2.24 of plastic stress concentration factor k_{cp}. The relation of measured static and dynamic yield strength and general yield forces has been determined. The simplified approach was used for calculation of local fracture stress σ_f from general yield force, applying the equation $\sigma_f = 106.F_{gy}$. Obtained values of local stress at fracture obtained by this way are summarised in Table 3.

(ii) For a range of CVN specimens tested statically in bending at one temperature tensile stress distributions below the V notch were calculated using FEM. The distances between the initiation origin and the notch root were measured from SEM micrographs. The distances were applied into calculated maximum tensile stress distributions and local stress corresponding to fracture was read. The separate values of local stress at fracture (σ_f (w)) have been evaluated supposing their behaviour according to Weibull statistics. The mean values are summarised in Table 3, the overview of data for the main investigated microstructures is available in Figure 7.

Table 3. CVN specimens, local fracture stresses σ_f, and characteristics of fractal dimension D_F

state labelling	thermal exposition	t_{gy} [°C]	σ_f [MPa]	σ_f (w) [MPa]	dominant failure micromechanism in initiation origin	D_F	standard deviation
A	initial	-140	2472	2475	cleavage	1.099	0.015
A & IA	embrittled by IA	-160	2185	-	cleavage – intergranular	1.093	0.018
A & SC	embrittled by SC	-120	2121	2261	cleavage – intergranular	-	-
R	initial	-145	2216	-	cleavage	-	-
R & SC	embrittled by SC	-65	1791	1735	intergranular	1.143	0.031

The results of both methods of critical stress determination are in a very good correlation. The main outcome of this evaluation can be seen in Figure 7 however.

The microstructural state of the steel A after step cooling treatment (A&SC, blue rhombi) possesses bi-modal behaviour of data. This practically means that two data sets differing in our case by predominant fracture initiation micromechanism have been taken into statistical calculation. As it has been confirmed by fractographic analysis the higher values of critical stress corresponded to more or less cleavage fracture mechanism, the lower values have been typical for intergranular fracture initiation. When differentiating the data according to predominant fracture initiation mechanism two mean values have been obtained. The first one, 2342 MPa, is value very close to cleavage fracture characteristics. The second one, 2121 MPa, appears to be more close to the most embrittled states of the steel A.

Testing the statistical features of the measured set of specimens and/or determined set of local fracture stress direct information about possible change in brittle fracture mechanism can be obtained.

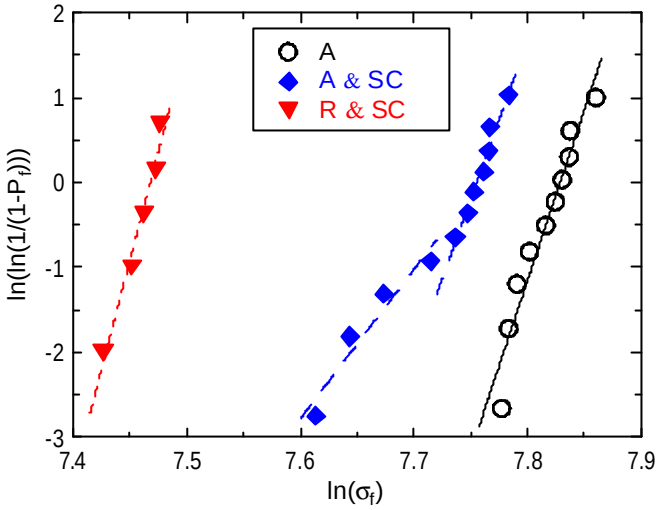

Figure 7. Rank probability diagram for critical stress values at fracture

Comparison of local fracture stress values (s_f) obtained for both steel melts and microstructures tested is shown Figure 8. This figure shows the relationships between the cleavage fracture stress, s_{CF}, controlling failure in un-embrittled microstructures and local fracture stress, s_C, controlling failure in embrittled microstructures. Both characteristics are here schematically plotted (full curves) into dependence on grain boundary enrichment (by impurity atoms). As grain boundary enrichment arbitrary quantity of "thermal exposition combined with the impurities level" could be applied characterising either cumulative exposition on temperatures (through tempering parameter etc.) or the chemical changes on grain boundaries (impurities atom enrichment etc.). A curve representing the change in cleavage fracture stress with tempering (without attracting impurity atoms to grain boundaries) is shown here (the decrease in cleavage fracture stress is connected with coarsening of carbides and matrix softening during thermal exposition). In case the local fracture stress s_f is above this curve the fracture could tend to be transgranular cleavage ($s_C > s_{CF}$), below this curve intergranular ($s_C < s_{CF}$).

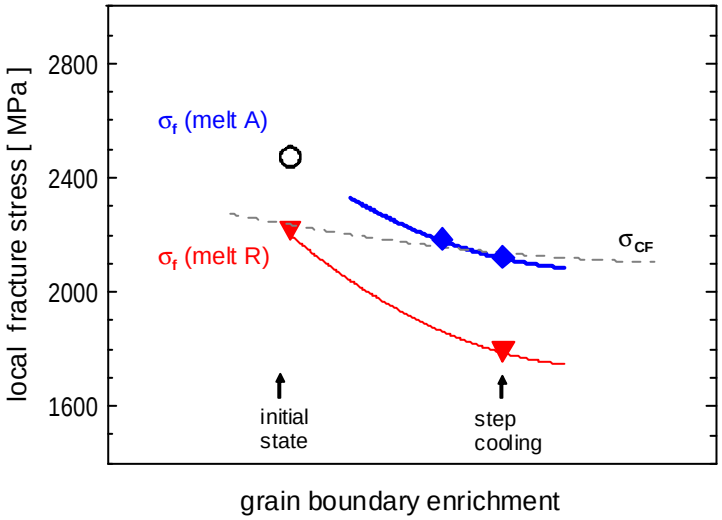

Figure 8.Effect of embrittling thermal exposition on critical fracture stress

From the change in critical stress corresponding to thermal exposition (ageing or step cooling) is evident that in steel with higher purity the local fracture stresses are comparably higher than for lower quality steel. For steel with good cleanliness (one

black empty circle and the blue upper full curve) the relatively high values of σ_f have been determined for initial state but also for conditions after embrittling treatment. Under the conditions of comparably stronger impurity enrichment of grain boundaries, the fracture is still controlled by cleavage rather than by intergranular decohesion. For steel with poor cleanliness two positions are characteristic for the change of local fracture stress σ_f (lower red full curve). The upper value of σ_f corresponds more to cleavage (σ_{CF}) the lower value more to intergranular fracture (σ_C).

Conclusions

Causes and characteristics governing the intergranular fracture initiation and occurrence of this fracture micromechanism in competition with cleavage one have been quantified in this work.

It has been found that the (local) fracture stress is lower for steel with intergranular initiation when compared to the steel with pure cleavage failure mechanism. From these observations follow that the fracture stress may be used as local criterion of fracture and as one of parameters for identification of critical impurity levels causing intergranular embrittlement.

Fractal dimension corresponded well to brittle fracture morphology reflecting on quite susceptible level the changes from pure cleave to intergranular fracture. A limit value corresponding to critical conversion of cleavage to intergranular fracture has been determined to be 1.12 . The cleavage fracture initiation morhphology has been typical by values of fractal dimension below this value. The fracture surfaces having fractal dimension higher were predominantly intergranular, with “critical” level of embrittlement.

Acknowledgments

Authors gratefully acknowledge to Grant Agency of the Academy of Sciences (GAAV 200410502) for the financial support.

References

1. Nutting, J.: *Ironmaking and Steelmaking*, **16**, No. 4, p. 219 (1989).
2. Briant, C. L., Banerji, S. K.: *Int. Metals Review*, 23, p. 164 (1978).
3. Kameda, J.: *Acta Metall*, **34**, p. 867 (1986).
4. Holzmann,. M., Man, J., Vlach, B. and Krumpos, J.: *Int. J. Pres. Ves. and Piping* , **57**, 141 (1994).
5. Pokluda, J., Šandera, P., Zeman, J.: *ASTM - STP 1131*, p. 653, (1992).
6. Mandziej, S.T.: *Scripta Met. at Mat.*, **27**, p. 793 (1992).
7. Dlouhý, I., Kozák, V., Válka, L., Holzmann, M.: *J. de Physique IV*, **C6 – 205**, 1996.
8. Man, J. Holzmann, M., Vlach, B.: *Zváranie (Welding)* , 32, p. 3, (1983).
9. Holzmann, M., Dlouhý, I., Vlach, B. & Krumpos , J.: *Int. J. Pres. Ves. and Piping*, 68, 99 (1996).
10. Nemec O., Stress Controlled Fracture Micromechanisms in Steels and Quantification of their Features, *PhD thesis*, VŠB - Technical University of Ostrava, (2004)
11. ASTM, E1921-02, 2002, *Standard Test Method for the Determination of Reference Temperature T_0 for Ferritic Steels in the Transition Range.*
12. Nemec, O. Holzmann, M., Dlouhý I.: In *Fraktography 2000*, Stará Lesná, p. 116.
13. Nemec, O, Dlouhý, I, Strnadel, B: The effect of crack propagation condition on fractal dimension of fracture surface *Metalic Mater*. **41**(3), p.177-192 (2003).